Equiangular Spiral Antenna Backed by a Shallow Cavity With Absorbing Strips

NAKANO, Hisamatsu / YAMAUCHI, Junji / IITSUKA, Yasushi / KIKKAWA, Katsuki
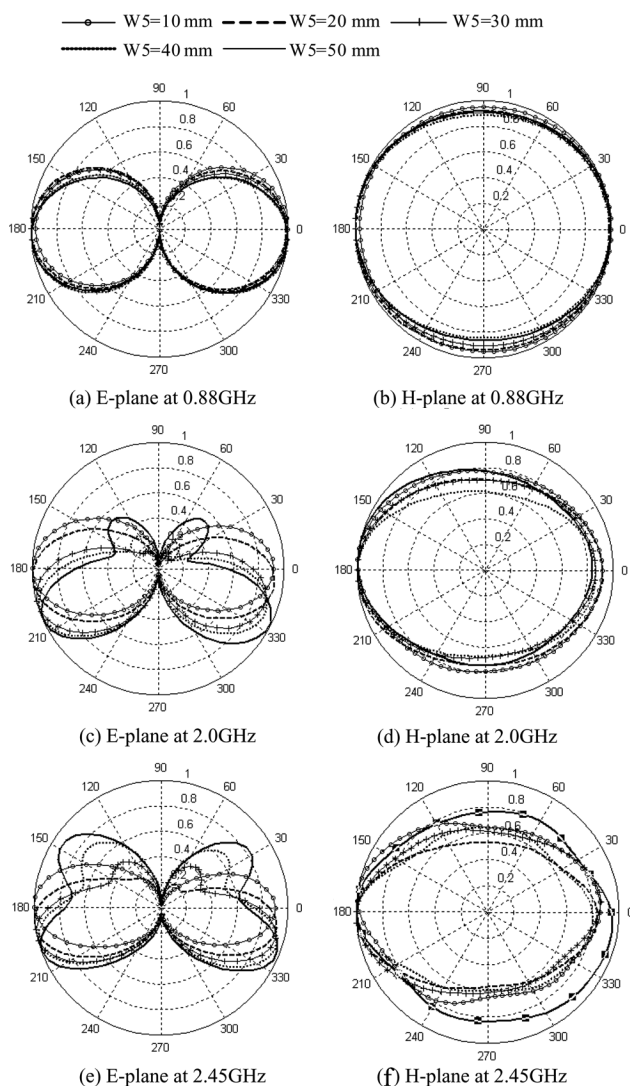
Fig. 9. Computed radiation patterns for various W5.

V. CONCLUSION

The proposed bow-tie is essentially a modified double-sided bow-tie. Two asymmetric arms are used to generate the beam tilt and overlapped to tune the operation band.

Different from the feed structures of previous bow-ties [1]–[7], the feed of proposed bow-tie is somewhat like the probe feed of a microstrip antenna. The grounded plane here serves as one arm of the bow-tie, and has an increasing dimension along the feed networks approaching the feed point. As a result, the feed cables behind the bow-tie may have some effects on the bow-tie performance. But the effects can be limited to an acceptable level by properly designing the feed networks with a relatively longer strip length (i.e., $W1 + W2$ in Fig. 1), as shown in this paper. Obviously, a bow-tie with feed networks of longer strip (thus feed point further from the overlapped ends) will suffers less from the effects of feed cable.

REFERENCES

[1] R. C. Compton, R. C. McPhedran, Z. Popovic, G. M. Rebeiz, P. P. Tone, and D. B. Rutledge, "Bow-tie antennas on a dielectric half-space: Theory and experiment," *IEEE Trans. Antennas Propag.*, vol. 35, pp. 622–631, Jun. 1987.
[2] Y. Lin and S. Tsai, "Coplanar waveguide-fed uniplanar bow-tie antenna," *IEEE Trans. Antennas Propag.*, vol. 45, pp. 305–306, Feb. 1997.
[3] Y.-D. Lin and S. N. Tsai, "Analysis and design of broadside-coupled stripline-fed bow-tie antennas," *IEEE Trans. Antennas Propag.*, vol. 46, no. 3, pp. 459–460, Mar. 1998.
[4] A. A. Eldek, A. Z. Elsherbeni, and C. E. Smith, "Wideband microstrip-fed printed bow-tie antenna for phased-array systems," *Microw. Opt. Technol. Lett*, vol. 43, no. 2, pp. 123–126, Oct. 2004.
[5] G. Zheng, A. A. Kishk, A. W. Glisson, and A. B. Yakovlev, "A broadband printed bow-tie antenna with a simplified balanced feed," *Microw. Opt. Tech. Lett.*, vol. 47, no. 6, pp. 534–536, Dec. 2005.
[6] G. Bindu, V. Hamsakkutty, A. Lonappan, J. Jacob, V. Thomas, C. K. Aanandan, and K. T. Mathew, "Wideband bow-tie antenna with coplanar stripline feed," *Microw. Opt. Technol. Lett*, vol. 42, no. 3, pp. 222–224, Jun. 2004.
[7] K. Kiminami, A. Hirata, and T. Shiozawa, "Double-sided printed bow-tie antenna for UWB communications," *IEEE Antennas Wireless Propag. Lett.*, vol. 3, pp. 152–153, 2004.

Equiangular Spiral Antenna Backed by a Shallow Cavity With Absorbing Strips

H. Nakano, K. Kikkawa, Y. Iitsuka, and J. Yamauchi

Abstract—When a conducting shallow cavity is placed behind an equiangular spiral to obtain a unidirectional beam, the inherent wideband characteristics of the spiral deteriorate. To restore the wideband characteristics, a ring-shaped absorbing strip (R-ABS) is placed under the spiral arms. Analysis of the equiangular spiral with the R-ABS is performed using the finite-difference time-domain method. It is found that the R-ABS successfully restores the wideband characteristics. Subsequently, the R-ABS is divided into two absorbing strips, each specified by an arc-angle ϕ_{ARC}. Analysis reveals that the radiation characteristics obtained using the R-ABS are reproduced when the arc-angle is greater than $\phi_{\mathrm{ARC}} = 90°$. Throughout this paper an extremely small cavity depth is selected for the analysis: 0.07 wavelength at the lower operating design frequency of 3 GHz.

Index Terms—Absorbing strips, cavity, equiangular spiral, wideband characteristics.

I. INTRODUCTION

A spiral element isolated in free space radiates a circularly polarized (CP) wave in the two directions normal to the spiral plane. This bi-directional radiation often must be transformed into unidirectional radiation when the spiral is used in point-to-point communication systems. So far, some investigations have been devoted to obtaining unidirectional radiation from an *Archimedean* spiral [1] backed by a conducting plane or a conducting cavity [2]–[6], [9].

This paper presents an approach for obtaining unidirectional radiation from a spiral element different from the Archimedean spiral: an *equiangular* spiral [7], where the spiral arms become wider as they extend. The equiangular spiral has a special advantage over the constant-width arm Archimedean spiral in that electronic devices can be installed on the wider arm sections of the equiangular spiral. This increases the potential for application of the spiral, and is an additional factor in encouraging research on the equiangular spiral. The equiangular spiral in this paper is backed by an extremely shallow cavity (the cavity depth/height is 7 mm, corresponding to 0.07 wavelength at the lower operating design frequency of 3 GHz).

First, a comparison of the antenna characteristics of the equiangular spiral with and without the cavity is presented. Subsequently, a ring-shaped absorbing strip (R-ABS) is added to the cavity and the effects of the R-ABS on the antenna characteristics are discussed. Finally, use of two arc-shaped absorbing strips (A-ABSs) in place of the R-ABS is proposed and the radiation characteristics are analyzed. The validity of the analysis results is confirmed with results from experimental work. Note that the reference of [8] provides data for a comparison of the equiangular spiral with the Archimedean spiral, both having absorbers. Also, note that a low-profile structure for spiral antennas radiating a unidirectional beam is discussed in [4], [9].

II. CONFIGURATION

Fig. 1(a) and (b) shows the exploded and side views of a two-arm equiangular spiral backed by a conducting cavity of height H_{cav} (= antenna height) and diameter D_{cav}. The spiral is supported by polystyrene foam material whose relative permittivity is $\varepsilon_r \approx 1$ (close to air). The two arms are symmetric with respect to the center and truncated at radial distance r_{max}. The edge $a - p_A$ is defined by radial distance $r = r_0 e^{a_s(\phi' + \pi/2)}$, where r_0 is a constant, a_s is the arm growth constant, and ϕ' is the winding angle, ranging from ϕ_{st} radians to ϕ_{end} radians. The edge $p_A - q_A$ is defined by a radius of $r_{max} = r_0 e^{a_s(\phi_{end} + \pi/2)}$. The edge $a' - q_A$ is described by rotating the edge $a - p_A$ by τ radians.

The upper operating frequency is limited by the feed structure near the antenna center, while the lower operating frequency as a CP antenna is determined by the antenna circumference, defined by $2\pi r_{max}$. Note that the antenna circumference $2\pi r_{max}$ must be chosen to be more than one wavelength at the lower operating frequency, taking the active region at this frequency [1] into consideration.

We design the antenna to operate within 3–9 GHz. For this, the lowest analysis frequency is chosen to be 2 GHz (below the lower operating design frequency of 3 GHz) and the highest analysis frequency is chosen to be 10 GHz (above the upper operating design frequency of 9 GHz). Preliminary calculations show that the radiation pattern has a depression around the z-axis when the antenna height (which always equals the cavity height H_{cav}) is half the wavelength, due to the image current created by the presence of the bottom conductor of the cavity. Based on this fact, the antenna is designed with a height of less than half the wavelength at the upper operating design frequency of 9 GHz; a value of $H_{cav} = 7$ mm is used as a test antenna height in this paper, corresponding to 0.21 wavelength at 9 GHz. Note that this antenna/cavity height H_{cav} is electrically small at low frequencies: 0.0467 wavelength at the lowest analysis frequency of 2 GHz and 0.07 wavelength at the lower operating design frequency of 3 GHz. The antenna configuration parameters are summarized in Table I. These remain the same throughout this paper.

III. ANALYSIS METHOD

The finite-difference time-domain method (FDTDM) [10] is used for analysis. The antenna structure shown in Fig. 1 is symmetric with
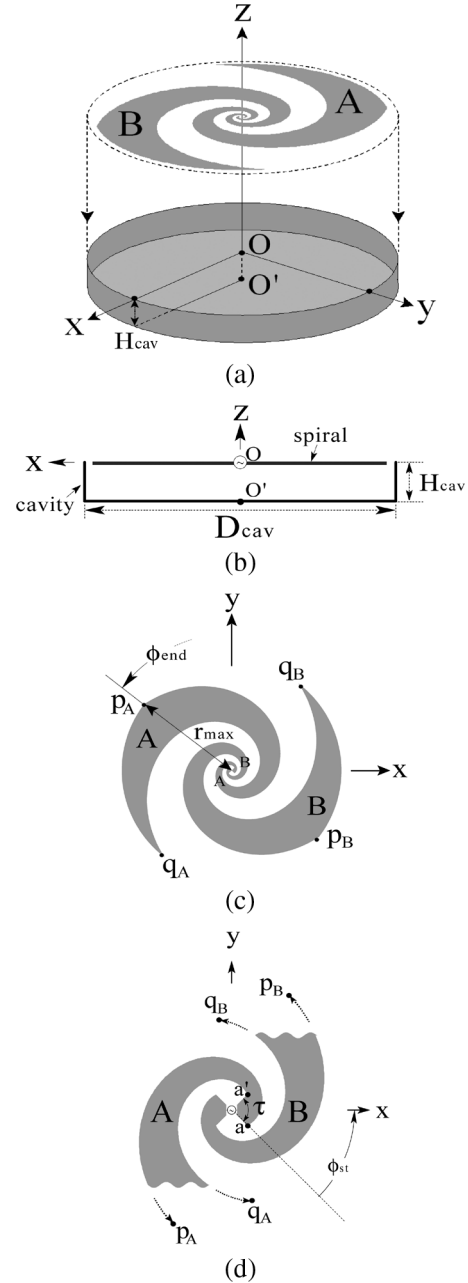

Fig. 1. Equiangular spiral antenna. (a) Exploded view. (b) Side view. (c) Conducting arms A and B. (d) Magnified view of the input region.

TABLE I
CONFIGURATION PARAMETERS

symbol	value	unit
r_0	1.5	mm
a_s	0.35	rad^{-1}
ϕ_{st}	-0.25π	rad
ϕ_{end}	2.806π	rad
τ	0.5π	rad
D_{cav}	120	mm
H_{cav}	7	mm

respect to the z-axis. The use of the structural symmetry reduces the computational burden for the FDTDM calculations.
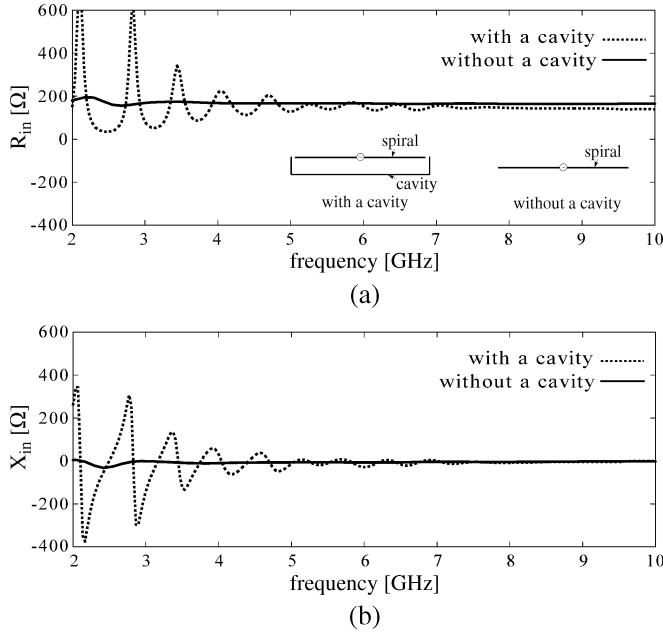
Fig. 2. Input impedance of an equiangular spiral antenna. (a) Input resistance R_{in}. (b) Input reactance X_{in}. The dotted lines are for the spiral with a cavity, and the solid lines are for the spiral without a cavity.
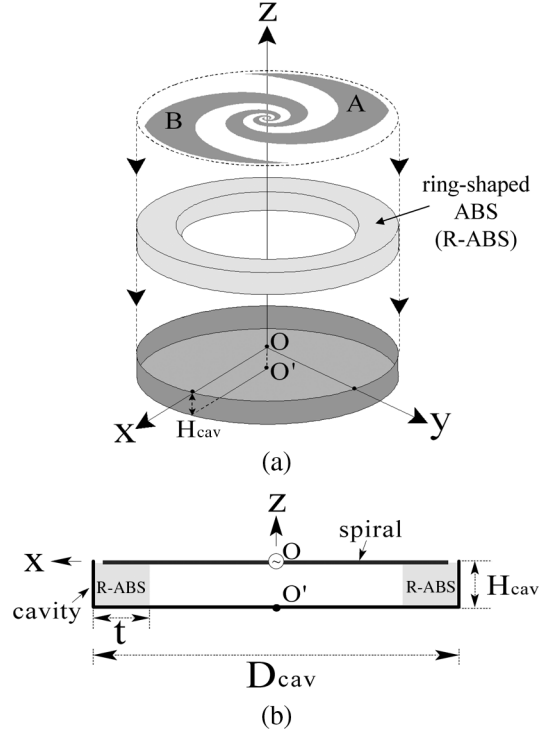

Fig. 3. Equiangular spiral with a ring-shaped absorbing strip. (a) Exploded view. (b) Side view.
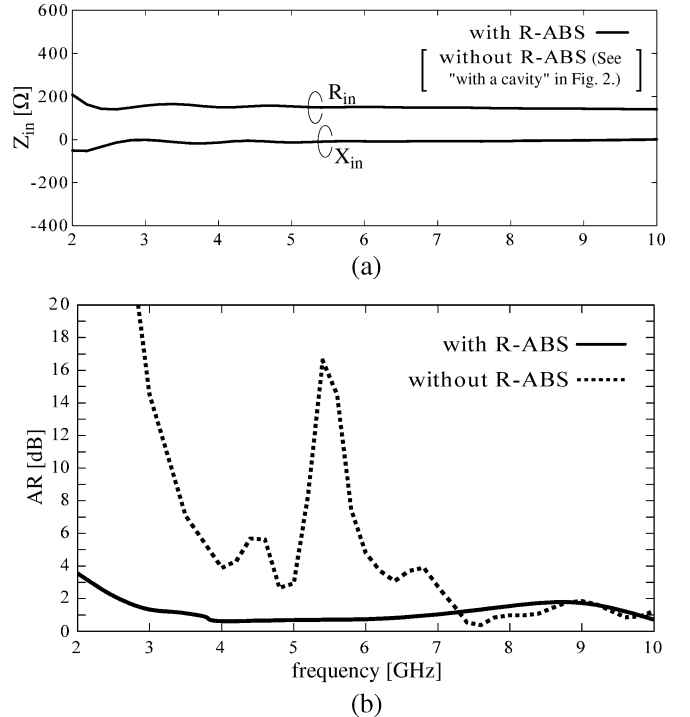

Fig. 4. Equiangular spiral. (a) Input impedance with a ring-shaped absorbing strip. (b) Axial ratios with and without a ring-shaped absorbing strip.

The radiation field is calculated using the equivalence principle [11]. For a CP antenna, the radiation field is decomposed into two components: a right-hand CP wave component E_R (complex value) and a left-hand CP wave component E_L (complex value). The absolute gain relative to a right-hand CP isotropic antenna, G_R, and the absolute gain relative to a left-hand CP isotropic antenna, G_L, are related to the axial ratio AR : $G_R = G/[1 + \{(AR \mp 1)/(AR \pm 1)\}^2]$ for $|E_R| > |E_L|$, where $G = \{(|E_\theta|^2 + |E_\phi|^2)/2Z_0\}/(P_{in}/4\pi r^2)$. Note that E_θ and E_ϕ are the radiation field components in the spherical coordinate system (r, θ, ϕ); $Z_0 = 120\pi$ ohms; and P_{in} is the power observed at the antenna center (not at the starting point of the feed line, where the power source is connected).

The calculations for the antenna characteristics are performed using programs written by the authors and run on a personal computer (3.2 GHz Pentium-D CPU with 2 GB of memory). When the cell size for the FDTDM is chosen to be $\Delta x = \Delta y = \Delta z = 0.5$ mm (= 0.005 wavelength at 3 GHz), calculation of the antenna characteristics at a single frequency (including the input impedance, axial ratio, radiation pattern, gain, and radiation efficiency) takes approximately 3.3 hours.

IV. ANALYSIS RESULTS AND DISCUSSION

A. Characteristics of an Equiangular Spiral Backed by a Cavity

The dotted lines in Fig. 2 show the input impedance components (resistance R_{in} and reactance X_{in}) of the cavity-backed equiangular spiral shown in Fig. 1. It is found that, as the frequency decreases (that is, the wavelength λ increases), variation in the input impedance becomes larger (note: when the wall of the cavity is removed and the spiral is backed by only the bottom conducting plane of the cavity, similar variation in the input impedance at low frequencies is observed). This is due to reflection of the electromagnetic (EM) fields at the bottom of the cavity; as the electrical antenna height H_{cav}/λ decreases, the reflected EM fields impinging on the spiral become stronger, affecting the current along the conducting spiral arms and resulting in the observed variation in the input impedance. Note that, for reference, the input impedance components for the equiangular spiral isolated in free space are shown by solid lines in this figure. Effects of the cavity on

the axial ratio are shown later [see Fig. 4(b), where deterioration in the axial ratio is illustrated].

If the antenna height H_{cav} is increased from the current test value (7 mm), the electrical antenna height H_{cav}/λ increases and the effect of the reflected EM fields on the current distribution along the spiral arms becomes weaker, resulting in less variation in the input impedance at low frequencies [12]. However, this goes against constructing a low-

profile antenna. In the next Section IV-B, we consider improvement of the deteriorated input impedance observed for the current test antenna height of $H_{cav} = 7$ mm, using absorbing material [9], [13].

B. Addition of a Ring-Shaped Absorbing Strip to the Cavity

The remaining current along the outermost arms (source of the EM fields reflected at the bottom of the cavity) is the cause of the variation in the input impedance at low frequencies. It is necessary to reduce or attenuate the reflected EM fields, in order for the antenna to operate over a wide frequency range. For this purpose, lossy material is applied [9], [13], as shown in Fig. 3, where a ring-shaped absorbing strip (R-ABS) of width t is placed under the antenna arms. The R-ABS is nonconducting dielectric material and specified by relative permittivity $\varepsilon_r (= \varepsilon' - j \varepsilon'')$ and relative permeability $\mu_r (= 1)$. Optimization of ε_r to widen the input impedance frequency response is performed using the real component, ranging from $\varepsilon' = 1.2$ to 3.1, with the loss tangent $(\tan \delta = \varepsilon''/\varepsilon')$ as a parameter. It is found that frequency-independent absorber material with $(\varepsilon', \tan \delta) = (1.9, 0.5)$ theoretically leads to a reasonable wideband input impedance. However, in practice, it is difficult to produce such frequency-independent absorber material. Therefore, we must choose absorber material that approximates the ideal values. In this case, we choose EM Absorber material, produced by TDK Corporation (model specification: ISFA); within the design frequency range of 3–9 GHz, ε' varies from $2.00(= 1.90 + 0.10)$ to $1.78(= 1.90 - 0.12)$ and $\tan \delta$ varies from $0.75(= 0.50 + 0.25)$ to $0.41(= 0.50 - 0.09)$,

Fig. 4(a) and (b) shows, respectively, the input impedance and axial ratio as a function of frequency, where the theoretical results illustrated by solid lines are obtained using the real parameters of the TDK ISFA EM Absorber material. As width t is increased, the radiation efficiency decreases at low frequencies; width t is optimized to be $t = 18$ mm at the lower operating design frequency of 3 GHz for a radiation efficiency criterion of 45%. It is found that the deterioration in the input impedance and axial ratio at low frequencies, observed for the spiral without the R-ABS, is ameliorated. Consequently, the equiangular spiral exhibits wideband characteristics. Note that the current distribution of the spiral without the R-ABS shows a standing wave at low frequencies, while that of the spiral with the R-ABS shows a traveling wave with gradual decay [14], which contributes to the wideband input impedance and axial ratio characteristics.

C. Use of Arc-Shaped Absorbing Strips in Place of the Ring-Shaped Absorbing Strip

The out-going current flowing from the feed point to the arm ends is reflected at the arm ends (q_A and q_B). This reflected current goes back toward the feed point as an in-coming wave. It is inferred that the antenna characteristics will not be greatly affected as long as the reflected current near the arm ends is absorbed. Based on this inference, we replace the R-ABS with two arc-absorbers (A-ABSs), each having an appropriate arc length [see Fig. 5, where the arc length is a function of arc-angle ϕ_{ARC}, measured from the arm end point (q_A or q_B)].

The first standing wave currents appearing near the arm ends are always above the A-ABSs having an arc-angle of 90° (within the design frequency range of 3–9 GHz). The FDTDM analysis results show that as the arc-angle is increased beyond $\phi_{ARC} = 90°$, the input impedance and axial ratio characteristics at low frequencies become similar to those obtained using the R-ABS (corresponding to $2\phi_{ARC} = 360°$) by virtue of sufficient absorption of the reflected current. Conversely, as the arc-angle is decreased below $\phi_{ARC} = 90°$, the antenna characteristics at low frequencies become noticeably different from those obtained when the R-ABS is used, due to insufficient absorption of the reflected current.
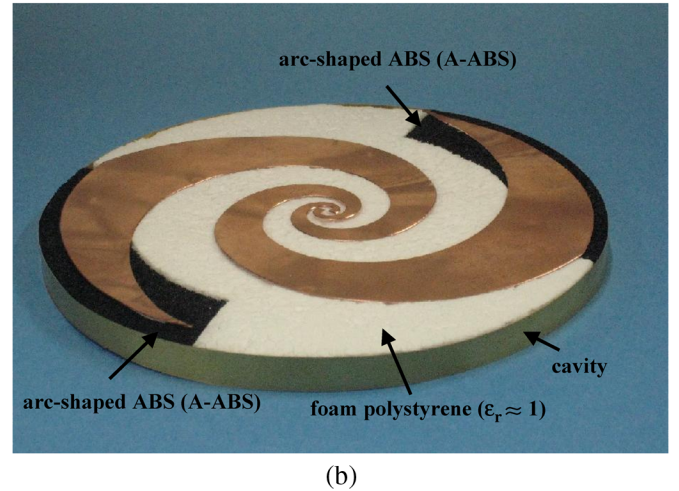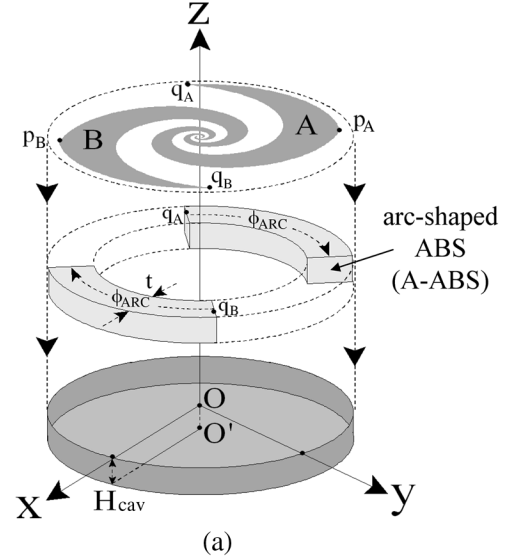

Fig. 5. Equiangular spiral with arc-shaped absorbing strips. (a) Exploded view. (b) Photo of experimental structure.

Fig. 6(a) and (b) shows the input impedance and axial ratio for $\phi_{ARC} = 90°$, respectively, together with the experimental results (white dots). For the experiment, a wideband balun that is perfectly frequency-independent is required for exciting the spiral. However, in reality, conventional baluns are not perfectly frequency-independent [15], [16]. Based on this fact, we use bazooka baluns [15] and check the validity of the theoretical results at frequencies of 2 GHz, 3 GHz, . . ., and 10 GHz. For practical use of this antenna, an appropriate small frequency-independent balun that can be installed inside the shallow cavity must be developed. This has yet to be done and is not described in this paper.

The radiation pattern for an arc-angle of $\phi_{ARC} = 90°$ is shown in Fig. 7(a), together with the radiation patterns for $\phi_{ARC} = 180°$ (corresponding to an R-ABS) and $\phi_{ARC} = 0°$ (corresponding to a cavity without the absorber), where the lower operating design frequency of 3 GHz is used. The spirals with the absorber radiate a CP wave in the z direction [see Fig. 7(a) and (b)], as desired. In contrast to these spirals with the absorber, a spiral without the absorber radiates a nearly linearly polarized wave [see Fig. 7(c)]. Note that the FDTDM results for $\phi_{ARC} = 90°$ are in good agreement with the experimental results, as shown in Fig. 7(a).
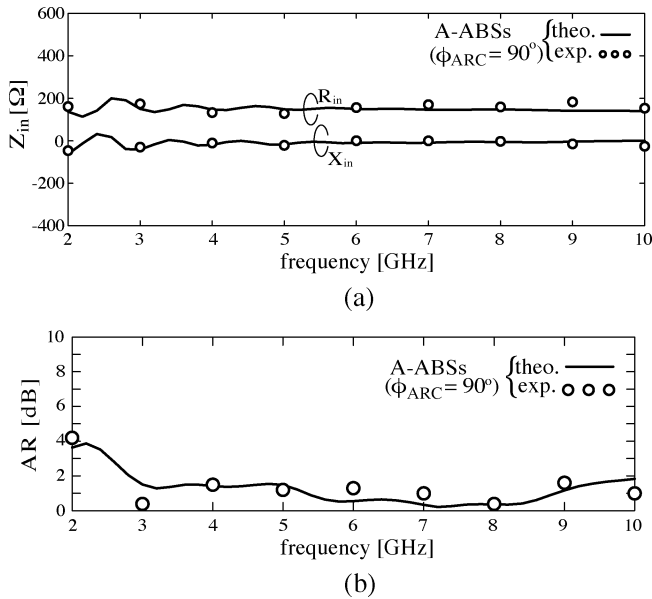
Fig. 6. Equiangular spiral with arc-shaped absorbing strips ($\phi_{ARC} = 90°$). (a) Input impedance. (b) Axial ratio.
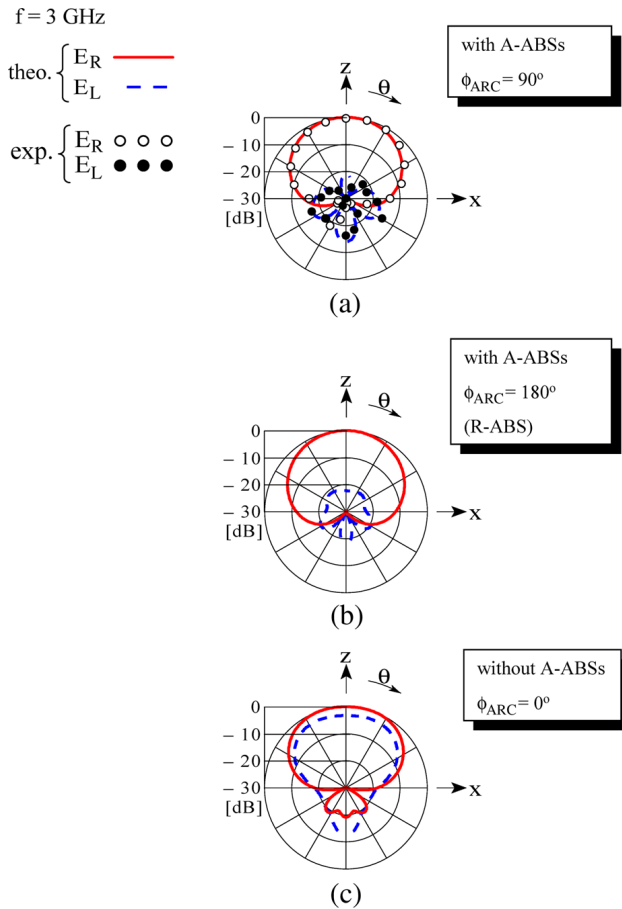

Fig. 7. Radiation patterns. (a) $\phi_{ARC} = 90°$. (b) $\phi_{ARC} = 180°$. (c) $\phi_{ARC} = 0°$.

As the frequency is decreased, absorption of the reflected EM fields increases and gain G_R decreases. When $\phi_{ARC} = 90°$, the gain is $G_R = 2.7$ dBi at the lowest analysis frequency of 2 GHz and increases

to 5.7 dBi at the lower operating design frequency of 3 GHz. At frequencies between the lower operating design frequency of 3 GHz and the upper operating design frequency of 9 GHz, the gain shows a relatively constant value: $G_R = 7.1 \pm 1.4$ dBi.

The variation in the gain (which is not significant) is related to the phase relationship between the primary and secondary radiation fields, where the primary radiation field is the wave (directly traveling in the $+z$ direction) from the spiral plane into free space, and the secondary radiation field is the wave that travels, first, in the $-z$ direction from the spiral plane toward the cavity, then is reflected by the conducting bottom of the cavity, and finally travels in the $+z$ direction, combining with the primary radiation field. The phase relationship between these two radiation fields varies with frequency (because the electrical length of the cavity, H_{cav}/λ, varies with frequency). Note that the effect of the fields reflected at the cavity bottom on the current distribution along the spiral arms varies with the electrical length H_{cav}/λ, as mentioned in Section IV-A; the change in the current distribution affects the phase relationship between the primary and secondary radiation fields; these two radiation fields add positively or negatively in free space with change in frequency, resulting in variation in the total radiation field and hence the gain. If the cavity is completely filled with absorbing material, the gain variation is quite small by virtue of disappearance of the effect of the secondary radiation field; however, the loss in the gain is significant (3 dB at its maximum) due to large absorption of the power input to the spiral.

The behavior of the gain for the spiral with A-ABSs is similar to that for the spiral with the R-ABS. Note that the gain at low frequencies increases as the antenna height H_{cav} is increased (although this goes against the objective of constructing a low-profile antenna). For example, a gain enhancement of 2 dB is obtained at the lowest analysis frequency of 2 GHz by increasing the antenna height from the current test height $H_{cav} = 7$ mm to $H_{cav} = 10.5$ mm.

From the above investigation, we find that the antenna characteristics, including the input impedance, axial ratio, radiation pattern, and gain, do not change significantly when the R-ABS is replaced with appropriately chosen A-ABSs.

V. CONCLUSIONS

An equiangular spiral antenna backed by a shallow conducting cavity is analyzed using the FDTDM. The cavity depth is chosen to be 0.07 wavelength at the lower operating design frequency of 3 GHz. The analysis shows that the inherent wideband input impedance obtained when the equiangular spiral is located in free space deteriorates when an extremely shallow cavity is added.

To restore the inherent wideband input impedance characteristic, a ring-shaped absorbing strip (R-ABS) is placed under the spiral arms. The analysis shows that the input impedance improves in the presence of this R-ABS. Subsequently, the R-ABS is divided into two same-sized, arc-shaped absorbers, each with arc-angle ϕ_{ARC} (the A-ABSs become an R-ABS when $2\phi_{ARC} = 360°$). It is revealed that the antenna characteristics when the arc-angle is greater than $\phi_{ARC} = 90°$ are similar to those when the R-ABS is used. The gain for $\phi_{ARC} = 90°$ shows a relatively constant value: $G_R = 7.1 \pm 1.4$ dBi within the design frequency range of 3 GHz to 9 GHz. It is concluded that adding an R-ABS or two A-ABSs is useful for forming a unidirectional radiation beam from an equiangular spiral backed by an extremely shallow cavity, while maintaining the wideband antenna characteristics.

REFERENCES

[1] J. A. Kaiser, "The Archimedean two-wire spiral antenna," *IRE Trans. Antennas Propag.*, vol. AP-8, pp. 312–323, May 1960.

[2] H. Nakano, K. Nogami, S. Arai, H. Mimaki, and J. Yamauchi, "A spiral antenna backed by a conducting plane reflector," *IEEE Trans. Antennas Propag.*, vol. AP–34, no. 6, pp. 791–796, June 1986.

[3] C. Penney and R. Luebbers, "Input impedance, radiation pattern, and radar cross section of spiral antenna using FDTD," *IEEE Trans. Antennas Propag.*, vol. 42, pp. 1328–1332, Sep. 1994.

[4] J. J. H. Wang, "The spiral as a traveling wave structure for broadband antenna applications," *Electromagnetics*, vol. 20, no. 4, pp. 323–342, Jul. 2000.

[5] J. L. Volakis, M. W. Nurnberger, and D. S. Filipovic, "A broadband cavity-backed slot spiral antenna," *IEEE Trans. Antennas Propag.*, vol. 43, no. 6, pp. 15–26, Dec. 2001.

[6] D. S. Filipovic and J. L. Volakis, "Novel slot spiral antenna designs for dual-band/multiband operation," *IEEE Trans. Antennas Propag.*, vol. 51, no. 3, pp. 430–440, March 2003.

[7] J. Dyson, "Equiangular spiral antenna," *IRE Trans. Antennas Propag.*, vol. 7, no. 2, pp. 181–187, Apr. 1959.

[8] R. Suzuki, R. Kobayashi, J. Yamauchi, and H. Nakano, "Terminal process of Archimedean spiral antenna," in *Proc. IEICE General Conf.*, Ishikawa, Japan, Sep. 2006, no. 1, p. 163.

[9] J. J. H. Wang and V. K. Tripp, "Design of multioctave spiral-mode microstrip antennas," *IEEE Trans. Antennas Propag.*, vol. 39, pp. 332–335, Mar. 1991.

[10] K. S. Yee, "Numerical solution of initial boundary value problems involving Maxwell's equations in isotropic media," *IEEE Trans. Antennas Propag.*, vol. AP-14, pp. 302–307, May 1966.

[11] R. Harrington, *Time-Harmonic Electromagnetic Fields*. New York: McGraw-Hill, 1961, pp. 106–110.

[12] W. Miyashita, K. Kikkawa, J. Yamauchi, and H. Nakano, "Cavity height characteristic of an equiangular spiral antenna," presented at the IEICE General Conf., Tottori, Japan, Sep. 2007, B-1-41.

[13] S. Lipsky, *Microwave Passive Direction Finding*. New York: Wiley-Interscience, 1987.

[14] K. Kikkawa, Y. Toma, J. Yamauchi, and H. Nakano, "Current distribution of a low-profile equiangular spiral antenna with strip absorber installed inside a cavity," in *Proc. IEICE General Conf.*, Fukuoka, Japan, Mar. 2008.

[15] R. C. Johnson and H. Jasik, *Antenna Engineering Handbook*, 2nd ed. New York: McGraw-Hill, 1984, pp. 43-23–43-31.

[16] R. Bawer and J. J. Wolfe, "A printed circuit balun for use with spiral antennas," *IEEE Trans. MTT*, vol. 8, no. 3, pp. 319–325, May 1960.

Novel Microstrip Antenna With Rotatable Patch Fed by Coaxial Line for Personal Handy-Phone System Units

Atsuya Ando, Kenichi Kagoshima, Akira Kondo, and Shuji Kubota

Abstract—An enhanced microstrip antenna is proposed that incorporates a patch that rotates around the inner conductor of the coaxial line or dielectric shaft and a novel coaxial line feeding technique that offers constant electromagnetic coupling. This proposal addresses the disadvantages in our previous patch antenna in which the resonant frequency diverges from the center frequency of the personal handy-phone system (PHS) band and the bandwidth decreases as the patch rotates because of the changing electromagnetic coupling between the patch and microstrip line due to the patch rotation. We verify that this enhanced patch antenna achieves the antenna gain of approximately 0 dBd, which is the same as that of the previously proposed antenna, while suffering no significant gain degradation due to unit inclination over inclination angles from $\pm 45°$ compared to a conventional quarter-wavelength whip antenna, which experiences a degradation of approximately 2.7 dB. We show that the maximum resonant frequency separation from the center frequency of the PHS band is reduced to 15 MHz from 31.4 MHz of the previous antenna using the novel coaxial line feeding technique. The effective bandwidth needed for PHS is achieved over the inclination angles of $-20°$ to $+40°$. Approximately 93% of the total bandwidth needed for PHS is achieved while the previous microstrip line type achieved only 58% coverage; accordingly, an adequate bandwidth for PHS use is obtained.

Index Terms—Electromagnetically coupled microstrip antenna, new coaxial line feeding technique, personal handy-phone system (PHS), rotatable patch antenna.

I. INTRODUCTION

In a previous paper [1], we proposed the novel electromagnetically coupled microstrip antenna with a rotatable patch to overcome the four main problems of whip antennas simultaneously: the effective gain degradation with unit inclination in land mobile propagation environments [2], the degradation experienced in effective antenna gain due to operator proximity [3], the RF exposure of the users [4], and antenna breakdown and poor handling. The previous paper described the structure of the newly developed antenna as installed in the actual units of the personal handy-phone system (PHS), showed the fundamental characteristics such as the radiation pattern, bandwidth, gain, and clarified the performance of the novel antenna in actual propagation environments.

Our original microstrip antenna has one disadvantage, the resonant frequency deviates from the center frequency of the PHS band as the patch rotates, and consequently, the effective bandwidth decreases as the patch rotates. This effect is due to the electromagnetic coupling between the patch and microstrip line changing with the patch rotation. This paper proposes an enhanced coaxial line feeding technique with constant electromagnetic coupling that eliminates this problem. It is verified that this novel microstrip antenna keeps the resonant frequency constant and improves the bandwidth performance enough to obtain sufficient bandwidth for PHS use.

The structure of the newly developed antenna installed in actual PHS units, is described. The performance of the novel antenna is investigated experimentally. The effectiveness of the novel feeding technique